

Violation of classical inequalities by photon frequency-filtering

C. Sánchez Muñoz, E. del Valle, C. Tejedor, and F.P. Laussy*

*Departamento de Física Teórica de la Materia Condensada and Condensed Matter Physics Center (IFIMAC),
Universidad Autónoma de Madrid, E-28049, Spain.*

(Dated: July 19, 2021)

The violation of the Cauchy–Schwarz and Bell inequalities ranks among the major evidences of the genuinely quantum nature of an emitter. We show that by dispensing from the usual approximation of mode correlations and studying directly correlations between the physical reality—the photons—these violations can be optimized. This is achieved by extending the concept of photon correlations to all frequencies in all the possible windows of detections, with no prejudice to the supposed origin of the photons. We identify the regions of quantum emission as rooted in collective de-excitation involving virtual states instead of, as previously assumed, cascaded transitions between real states.

PACS numbers: 42.50.Ct, 42.50.Ar, 42.50.Pq

INTRODUCTION

Classical descriptions of the electromagnetic field [1] and local hidden variable theories [2] yield a series of inequalities that impose an upper limit to the correlations between two modes and whose violation prove unequivocally the non-classical character of quantum mechanics [3]. Among such equalities, the Cauchy–Schwarz inequality and Bell’s inequalities are prominent examples that have been put to scrutiny in a large and varied set of platforms. The Cauchy–Schwarz Inequality (CSI) [4] is one of the most important relations in all of mathematics. It states that fluctuations of products of random variables are bounded by the product of autocorrelations: $|\langle XY \rangle| \leq \sqrt{\langle X^2 \rangle \langle Y^2 \rangle}$. When X and Y are quantum observables, however, this relation can be violated. That is to say, quantum correlations between two objects can be so strong as to overcome their individual fluctuations in a way that is unaccountable by classical physics. Bell’s inequalities (BI), on the other hand, refer to the wider problem of the nonlocal character of quantum mechanics [5]. Their violation decides in favour of quantum theory over local hidden variable theories. The underlying correlations are well known to power quantum information processing [6].

The first experimental demonstrations of violation of these inequalities were realized in the 70s in the radiation of an atomic two-photon cascade for the CSI [7] and in the early 80s for the BI [8, 9]. There has been a large body of literature confirming and documenting such violations ever since [10–16]. Most experimental realizations in both cases involve the correlation of photons of different frequencies emitted in a multi-photon process, such as atomic cascades [8] or four-wave mixing [13, 17]. While in the underlying theoretical models these photons are attributed to quantum modes corresponding to specific optical transitions [3], the only physical reality perceived by the measuring devices are the photons themselves. One can therefore inquire what are the correlations between photons with a given property—typically, frequency and

polarization for CSI and BI respectively—with no theoretical prejudice as to their origin. In this text, we address this question in a general context for frequency correlations, but to fix ideas, we will illustrate our claims on one particular source of photons. To emphasize that the frequency-correlated photons do not need to be attached to different modes, we will consider a single-mode emitter. The simplest non-trivial candidate—resonance fluorescence—is also of great intrinsic interest and has been a favourite testbed of quantum optics [18].

FREQUENCY CORRELATIONS IN RESONANCE FLUORESCENCE

Resonance fluorescence refers to the light emitted under strong coherent driving by a two-level system (2LS) [19–21]. At high pumping intensity, the luminescence spectrum splits into three peaks, known as the Mollow triplet [22] (cf. Fig. 1(a)). While the emission comes from a single mode, σ , the distinctive spectral shape calls naturally to question what are the correlations of—and between—the three peaks. It has been suggested theoretically [23–26] and established experimentally [25, 27, 28] that the photons from the peaks are strongly correlated. The Hamiltonian for this system reads:

$$H_0 = \omega_\sigma \sigma^\dagger \sigma + \Omega (e^{-i\omega_L t} \sigma^\dagger + e^{i\omega_L t} \sigma) \quad (1)$$

with ω_σ the energy of the 2LS and Ω the intensity of the field driving it with frequency ω_L . With little loss of generality we will consider resonant excitation: $\omega_L = \omega_\sigma$. Dissipation for the emitter is included in the density matrix formalism as a Lindblad term $\mathcal{L}_\sigma \rho$ with decay rate γ_σ in the master equation [29]:

$$\dot{\rho} = -i[H_0, \rho] + \frac{\gamma_\sigma}{2} \mathcal{L}_\sigma \rho \quad (2)$$

where $\mathcal{L}_\sigma \rho = 2\sigma\rho\sigma^\dagger - \sigma^\dagger\sigma\rho - \rho\sigma^\dagger\sigma$. One can solve this equation to obtain an analytical expression of the spectrum featuring the Mollow triplet [22, 30], which at

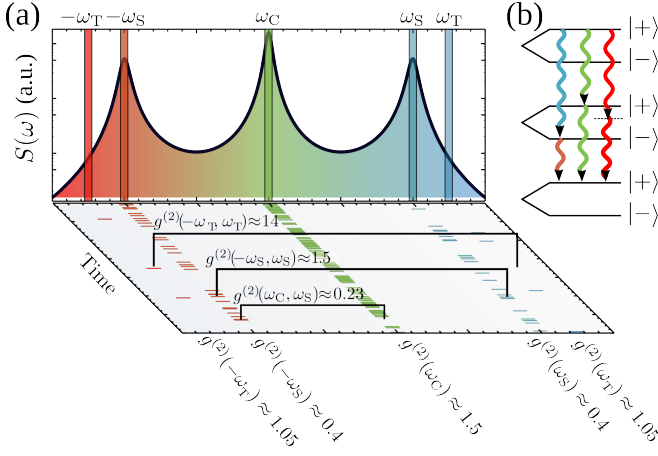


FIG. 1: (Color online) Violation of CSI and BI by frequency-resolved correlations. (a) Spectrum of resonance fluorescence, where filtering is illustrated in the tails (T), sidebands (S) and central peak (C) of the Mollow triplet. (b) Two-photon de-excitation between rungs of the Mollow ladder involve an intermediate real state (blue, orange and green arrows) or a virtual state (red arrows). The latter type conveys CSI and BI violation. It is found in the flanks or between the peaks, where the signal is however weaker. Parameters: $\Omega = 10\gamma_\sigma$, $\Gamma = \gamma_\sigma$, $\omega_S \approx 2\Omega$, $\omega_T = 2.5\Omega$.

resonance presents a central peak and two sidebands at $\omega = \omega_L \pm \omega_S$, where

$$\omega_S = \Re\{\sqrt{(2\Omega)^2 - (\gamma_\sigma/4)^2}\}. \quad (3)$$

At this point, an ad hoc multiple-mode description is usually enforced out of the genuine single mode σ which, dressed by the laser, yields three types of transitions between the dressed states $|\pm\rangle$ (cf. Fig. 1(b)). This allows to introduce three auxiliary modes, associated to the three peaks: $\sigma_1 = c^2|-\rangle\langle+|$, $\sigma_2 = cs[|+\rangle\langle+| - |-\rangle\langle-|]$ and $\sigma_3 = -s^2|+\rangle\langle-|$ with s and c two amplitudes [24, 26]. One can easily compute correlations $\langle\sigma_i^\dagger\sigma_j^\dagger\sigma_j\sigma_i\rangle$ for $1 \leq i, j \leq 3$ between these modes, that are associated in the input/output formalism to those $\langle a_i^\dagger a_j^\dagger a_j a_i \rangle$ of the detected photons with a given frequency [31].

There are various shortcomings to this approach, which is an approximation rooted in the physical picture of the dressed atom. First, the identification of each photon to a given transition based on its frequency is a simplification. Although infrequent, it happens that a photon detected at the frequency of a given peak actually originates from the transition that chiefly accounts for another peak. When considering regions of overlap, such a misattribution can become a source of large errors. Second, this approach neglects interferences between photons that truly are emitted by the same mode σ . Third, modes defined in this way are usually non-commuting, and therefore correlations at zero delay can yield different results depending on the order of the operators [25].

Finally, this approach also restricts the calculation to the three modes thus defined, while one can correlate any two frequency windows, of various widths and centered at arbitrary frequencies, not compulsorily at the peak maxima.

THEORY OF FREQUENCY CORRELATIONS

To dispense from these approximations and constraints, an exact theory of frequency-resolved photon detection is required to correlate any two photons based only on their measured properties, with no assumption as to their origin or time of emission. The formal expression for the second-order correlation function between photons of two different frequencies without recouring to contrived modes has been formalized in the late 80s [32, 33]. We will denote it $g_\Gamma^{(2)}(\omega_1, \omega_2)$. It provides the statistics of photons with frequencies ω_1 and ω_2 spectrally filtered in a Lorentzian window of width Γ . The resulting integral form turns out to be so awkward, however, that even in the possession of the expression, there was the need to come back to the multi-mode approximation to compute it. In this text, we recourse to del Valle *et al.*'s theory of frequency-resolved photon correlations [34] to compute exactly this measurable property, with no intermediate artificial modes and, therefore, taking into account all the possible interferences and indistinguishability imposed by quantum mechanics. This theory establishes that frequency-resolved correlations of the light emitted by any open quantum-system are the same as the correlations between “sensors” at these frequencies. These sensors are bosonic, commuting modes with annihilation operator a_i , $i = 1, 2$, free energy ω_i and decay rate Γ —accounting for the frequency linewidth of the sensors—that are weakly coupled to the emitting mode with a small coupling constant ε . They are included in the dynamics by the Hamiltonian term $H_S = \sum_i \omega_i a_i^\dagger a_i + \varepsilon(a_i^\dagger \sigma + a_i \sigma^\dagger)$ and Lindblad terms $\frac{\Gamma}{2} \sum_i \mathcal{L}_{a_i} \rho$ [34]. Frequency-resolved correlations are then computed as:

$$g_\Gamma^{(2)}(\omega_1, \omega_2) = \lim_{\varepsilon \rightarrow 0} \frac{\langle a_1^\dagger a_2^\dagger a_1 a_2 \rangle}{\langle a_1^\dagger a_1 \rangle \langle a_2^\dagger a_2 \rangle}. \quad (4)$$

With such a theoretical apparatus, a full mapping of the photon correlations can be obtained. For the case of the Mollow triplet that we have chosen for illustration, the problem takes the vivid form pictured in Fig. 1. The spectral shape—the triplet—is represented in log scale with a choice of five frequency windows, centered at $\pm\omega_T$ (tails), $\pm\omega_S$ (sidebands) and ω_C (central peak). A quantum Monte Carlo trajectory was calculated to simulate the photon-detection events [35] for photo-detectors measuring in these windows. The emitted photons in a small fraction of the trajectory are represented with ticks on

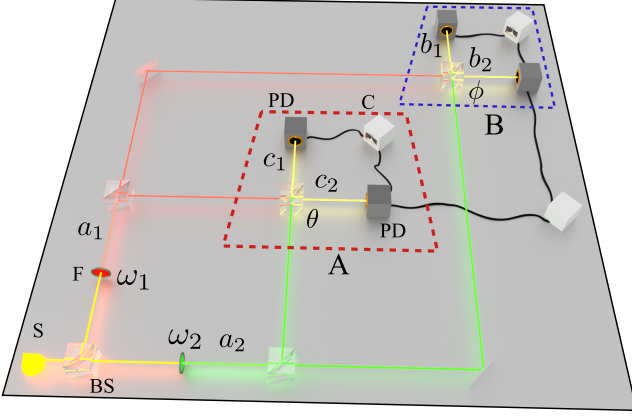


FIG. 2: (Color online) Test for the violation of Bell inequalities by frequency filtering. A source (S) emits photons in a broadband of frequencies. Frequency filters (F) select light at frequencies ω_1 and ω_2 , described by the operators a_1 and a_2 . Recombination at beam splitters (BS) with transmittivities given by $\sin \theta$ and $\sin \phi$ gives a total of four output beams, which are collected at the photodetectors (PD) and correlated with coincidence counters (C). Alice (A) and Bob (B) test nonlocality by independently measuring probability of detection at the output ports of the two beam splitters, $P_{\pm}^{A\theta}$ and $P_{\pm}^{B\phi}$.

the projected plane of Fig. 1(a). The intensities vary in each frequency window: there is of course more signal in the central peak than in the sidebands and more so than in the tails. What is of interest in quantum optics is the statistical distribution of, and the correlation between, these photons. The auto-correlation in a given window, shown in the lower part of Fig. 1(a), gives the statistics of emission of the stream of photons now defined by their mean frequency and spread. While the light emitted by the two-level system overall is perfectly antibunched, one sees that by spectral filtering, one can “distill” light with different statistical properties [36], namely, i) uncorrelated in the tails, ii) antibunched in the satellite peaks and iii) bunched in the central peak. One can similarly calculate the cross-correlations between photons from two different windows, showing this time that photons from the satellites are positively correlated, $g_{\Gamma}^{(2)}(-\omega_S, \omega_S) \approx 1.5$, while photons from one satellite and the central peak are anti-correlated, with $g_{\Gamma}^{(2)}(\omega_C, \omega_S) \approx 0.23$. It is worth noting here that the stronger correlations come from the tail events, with $g_{\Gamma}^{(2)}(-\omega_T, \omega_T) \approx 14$ for the window chosen, and increasing with greater still separations. The price to pay for these strong correlations is a correspondingly vanishing signal. Events are more rare but the strength of their correlations is increased. This is a general trend.

VIOLATION OF CAUCHY-SCHWARZ AND BELL’S INEQUALITIES BY FREQUENCY FILTERING

In a quantum optical context, Cauchy-Schwarz and Bell’s inequalities can be expressed through the correlators $\langle a_i^\dagger a_j^\dagger a_j a_i \rangle$, with $i, j \in \{1, 2\}$, of two electromagnetic modes a_1 and a_2 . In terms of Glauber’s second-order correlation functions at zero delay $g_{ij}^{(2)} = \langle a_i^\dagger a_j^\dagger a_j a_i \rangle / (\langle a_j^\dagger a_j \rangle \langle a_i^\dagger a_i \rangle)$ [37], the CSI reads $[g_{12}^{(2)}]^2 \leq g_{11}^{(2)} g_{22}^{(2)}$. This can be expressed in terms of a ratio R that quantifies the degree of CSI violation:

$$R = [g_{12}^{(2)}]^2 / [g_{11}^{(2)} g_{22}^{(2)}] \quad (5)$$

so the CSI takes the form:

$$R \leq 1. \quad (6)$$

One can use the definition (4) for the cross correlations of Eq. (5) to obtain a degree of CSI violation for frequency filtered light, $R_{\Gamma}(\omega_1, \omega_2)$.

The case of BI is less straightforward but can be cast in the same form. In the CHSH framework [38], one considers correlated pairs of particles. One of these particles enters an apparatus where an observable A_θ is measured while the other particle enters another apparatus where an observable B_ϕ is measured. θ and ϕ are adjustable parameters of the apparatuses, i.e., a polarization angle. The results of each measurement must be dichotomic, i.e., in each apparatus, the particle must select one of two possible channels of the observables, providing values ± 1 (in some units) with probabilities $P_{\pm}^{(A_\theta)}$ and $P_{\pm}^{(B_\phi)}$, respectively. Therefore, the measurement in each apparatus yields the mean values $\langle A_\theta \rangle = P_+^{(A_\theta)} - P_-^{(A_\theta)}$ and $\langle B_\phi \rangle = P_+^{(B_\phi)} - P_-^{(B_\phi)}$. As a consequence of this dichotomic character, the correlation $E(\theta, \phi) = \langle A_\theta B_\phi \rangle$ between both observables reads:

$$E(\theta, \phi) = P_{++}^{(A_\theta, B_\phi)} + P_{--}^{(A_\theta, B_\phi)} - P_{+-}^{(A_\theta, B_\phi)} - P_{-+}^{(A_\theta, B_\phi)}, \quad (7)$$

where $P_{\pm\pm}^{(A_\theta, B_\phi)}$ is the joint probability of measuring $A_\phi = \pm 1$ and $B_\phi = \pm 1$. From this expression in a local hidden-variable theory, one can derive a BI in the CHSH form [3, 38]:

$$B \leq 2 \quad (8)$$

where

$$B = |E(\theta, \phi) - E(\theta, \phi') + E(\theta', \phi') + E(\theta', \phi)|. \quad (9)$$

To clarify these concepts, we first consider the case usually discussed in which the particles being correlated are photons and the measurements are done in the polarization degree of freedom. By the nature of the observable,

$P_{\pm}^{(A_{\theta})}$ corresponds to the fraction of the total intensity at both output arms of a polarizing beam splitter:

$$P_{\pm}^{A_{\theta}} = \langle I_{\pm}^{(A_{\theta})} \rangle / \langle I_{+}^{(A_{\theta})} + I_{-}^{(A_{\theta})} \rangle, \quad (10)$$

where the adjustable parameter θ corresponds to the polarization angle. Correspondingly, the joint probability reads:

$$P_{\pm\mp}^{A_{\theta}, B_{\phi}} = \frac{\langle I_{\pm}^{(A_{\theta})} I_{\mp}^{(B_{\phi})} \rangle}{\langle (I_{+}^{(A_{\theta})} + I_{-}^{(A_{\theta})})(I_{+}^{(B_{\phi})} + I_{-}^{(B_{\phi})}) \rangle}, \quad (11)$$

and therefore, we can write $E(\theta, \phi)$ as:

$$E(\theta, \phi) = \frac{\langle (I_{+}^{(A_{\theta})} - I_{-}^{(A_{\theta})})(I_{+}^{(B_{\phi})} - I_{-}^{(B_{\phi})}) \rangle}{\langle (I_{+}^{(A_{\theta})} + I_{-}^{(A_{\theta})})(I_{+}^{(B_{\phi})} + I_{-}^{(B_{\phi})}) \rangle}. \quad (12)$$

This is the typical situation when measuring BI violations for states of the type:

$$|\psi\rangle = \frac{1}{\sqrt{2}}(a_{1+}^{\dagger}a_{2+}^{\dagger} + a_{1-}^{\dagger}a_{2-}^{\dagger})|0\rangle, \quad (13)$$

where $a_{i,\pm}^{\dagger}$ is the creation operator for a photon with polarization \pm along path i , i.e., for states that are entangled.

In our work, we focus on the correlations from the output of a dynamical process, that is, we do not restrict to deterministic pure states [3] but consider a steady state as an input. This means that the intensities $I_{\pm}^{(A_{\theta}/B_{\phi})}$ are no restricted to unity but can take any positive value. Moreover, we focus on a different scenario that does not involve the polarization degree of freedom, but only two modes states of the type $|\psi\rangle = a_1^{\dagger}a_2^{\dagger}|0\rangle$. If disposing of an emitter that provides such a two-mode output, it is immediate to bring it into an entangled form

$$|\psi\rangle = \frac{1}{2}(a_{1+}^{\dagger}a_{2+}^{\dagger} - a_{1-}^{\dagger}a_{2-}^{\dagger} + ia_{1+}^{\dagger}a_{2+}^{\dagger} + ia_{1-}^{\dagger}a_{2-}^{\dagger})|0\rangle \quad (14)$$

by placing two beam splitters across paths 1 and 2. Subscripts \pm then refer to path instead of polarization. By recombining the four resulting beams in two additional beam splitters with variable transmitivities, that act as the apparatuses measuring A_{θ} and B_{ϕ} , these states can also violate the BI by following the same line of reasoning as exposed above [3, 38]. θ and ϕ represent in this case the tunable transmitivities of the two final beam splitters.

The setup implementing such a scheme of BI based on frequency filtering is sketched in Fig. 2, where the path degree of freedom 1, 2 is associated to the energy degree of freedom ω_1, ω_2 by using frequency filters. The two possible channels of detection in each final beam splitter are then equivalent to the two output ports of the polarizing filters of the conventional case, and the arguments that

led to Eqs. (10) and (11) apply similarly. In a quantum-mechanical treatment, the modes at the output arms of the beam splitters are given by:

$$\begin{aligned} c_1 &= \cos \theta a_1 + \sin \theta a_2, & c_2 &= -\sin \theta a_1 + \cos \theta a_2, \\ b_1 &= \cos \phi a_1 - \sin \phi a_2, & b_2 &= \sin \phi a_1 + \cos \phi a_2, \end{aligned} \quad (15)$$

and $E(\theta, \phi)$ takes the form:

$$E(\theta, \phi) = \frac{\langle (c_1^{\dagger}c_1 - c_2^{\dagger}c_2)(b_1^{\dagger}b_1 - b_2^{\dagger}b_2) \rangle}{\langle (c_1^{\dagger}c_1 + c_2^{\dagger}c_2)(b_1^{\dagger}b_1 + b_2^{\dagger}b_2) \rangle}. \quad (16)$$

We adopt the standard choice of angles that provides the greatest violation of the inequality: $\theta = 0$, $\phi = \pi/8$, $\theta' = \pi/4$, $\phi' = 3\pi/8$. This yields the following expression for B :

$$B = \sqrt{2} \left| \frac{\langle a_1^{\dagger 2}a_1^2 \rangle + \langle a_2^{\dagger 2}a_2^2 \rangle - 4\langle a_1^{\dagger}a_2^{\dagger}a_1a_2 \rangle - \langle a_1^{\dagger 2}a_2^2 \rangle - \langle a_2^{\dagger 2}a_1^2 \rangle}{\langle a_1^{\dagger 2}a_1^2 \rangle + \langle a_2^{\dagger 2}a_2^2 \rangle + 2\langle a_1^{\dagger}a_2^{\dagger}a_1a_2 \rangle} \right|. \quad (17)$$

It is equally easy to formulate these concepts in terms of frequency correlations than for the CSI. The operators a_1 and a_2 in Eq. (15) can be replaced by the sensor operators previously introduced and employed into Eq. (4), thus describing the light emitted at the two frequencies ω_1 and ω_2 , as shown in Fig. 2. Direct application of Eq. (17) with these sensors a_i , whose finite linewidth Γ is described by their decay rate, provides $B_{\Gamma}(\omega_1, \omega_2)$.

RESULTS

At this point, we have set the stage to fully characterize the quantumness of the emission in terms of violation of the CSI and BI spanning over all the frequencies of emission and windows of detection. Note the considerable improvement as compared to the mode-correlation approach, since a continuum of frequencies in windows of arbitrary sizes can now be investigated without assumptions on the order of emission. Figure 3 shows three correlation landscapes in the frequency domain depicting the value of $g_{\Gamma}^{(2)}(\omega_1, \omega_2)$, $R_{\Gamma}(\omega_1, \omega_2)$ and $B_{\Gamma}(\omega_1, \omega_2)$ for three different values of the detector linewidth in an otherwise identical configuration. An animation of the full landscapes of correlations as a function of the linewidth of filtering is provided in the Supplemental Material. It immediately comes across that the quantum character of the emission, where the inequalities are violated, is structured along three antidiagonals. In particular, the anticorrelation $g_{\Gamma}^{(2)}(\omega_1, \omega_2) < 1$ (corresponding to blue areas in Fig. 3(a)), is a CSI violation in time when $\omega_1 = \omega_2$ and therefore corresponds to a non-classical effect [39]. It makes no such guarantee, however, of a genuine quantum nature when $\omega_1 \neq \omega_2$, and could in fact even be produced by a classical emitter [40]. The corresponding CSI violation in time in this case is $\left[g_{\Gamma}^{(2)}(\tau, \omega_1, \omega_2) \right]^2 > g_{\Gamma}^{(2)}(0, \omega_1, \omega_1)g_{\Gamma}^{(2)}(0, \omega_2, \omega_2)$, which

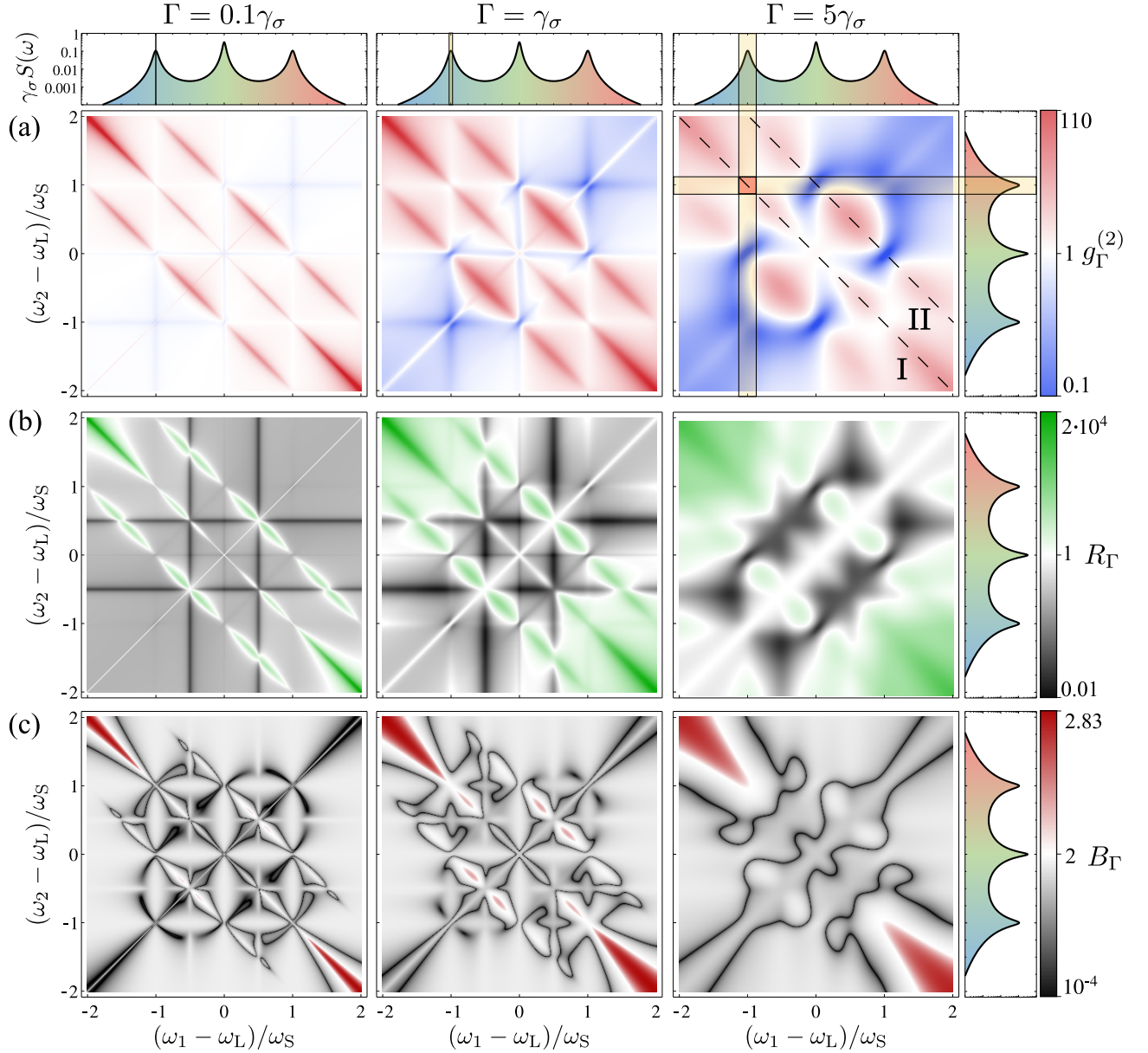


FIG. 3: Landscapes of correlations in the frequency domain for three different filter linewidths. (a) $g_{\Gamma}^{(2)}(\omega_1, \omega_2)$, (b) $R_{\Gamma}(\omega_1, \omega_2)$ and (c) $B_{\Gamma}(\omega_1, \omega_2)$. In (b) [resp. (c)], the color code is such that green [resp. red] violates the CSI [resp. BI] and thus corresponds to genuine quantum correlations between the detected photons in the corresponding energy windows, while black and white do not (with white maximizing the inequality). The violation originates from the emission that involves virtual states. Dashed lines I and II in (a) are the cuts in the frequency domain along which curves in Fig. 4 are calculated. The spectra on the axes show which frequency windows are correlated. Parameters are the same as in Fig. 1. An animation of these landscapes as a function of the detector linewidth is provided in the Supplemental Material.

we study at zero time delay $\tau = 0$. This shows the necessity to turn to such tests to assess the quantum character of an emitter by frequency filtering. The regions where they are violated indeed correspond not to frequency antibunching but, on the opposite, to frequency bunching in the two-photon correlation spectrum. The reason for this lies in the nature of the violation, with cross-correlations being higher with respect to auto-correlations than permitted by classical physics. Physically, the anti-diagonals

where this happens are precisely those where two-photon emission occurs in a “leapfrog process” [41], i.e., a jump over the intermediate real state by involving a virtual state instead. This generates the state $|11\rangle$ that, fed to beam splitters, generates the maximally entangled state that optimizes the violation. The anti-diagonal, line I, corresponds to transitions from $|+\rangle$ to $|+\rangle$ or from $|-\rangle$ to $|-\rangle$, two rungs below, as is sketched in Fig. 1(b), thus satisfying $\omega_1 + \omega_2 = 0$. Line II and its symmetric cor-

respond to transitions from $|+\rangle$ to $|-\rangle$ and from $|-\rangle$ to $|+\rangle$, respectively, satisfying $\omega_1 + \omega_2 = \pm\omega_S$. The CSI and BI are less, or are not, violated whenever the intermediate rung intersects a real state, as seen by the fact that the green (for R_Γ) and red (for B_Γ) regions are depleted or pierced when intersecting the sidebands $\pm\omega_S$. This is particularly important since previous studies focused precisely on correlations between real transitions, i.e., between peaks, such as indicated by the red square in the rightmost panel of Fig. 3(a). Instead, the exact treatment shows that these are detrimental to the effect, that is optimum when involving virtual states, since these are the vector of quantum correlations. It is easy to prove, from the closed form expression Eqs. (6–8) in Ref. [41], that a single-mode emitter with no dressing (here by the laser) never violates the CSI, regardless of frequencies and detection widths. The same was checked numerically for the case of BI. Notably, this is true even if the emitter is a two-level system and exhibits perfect antibunching, $g^{(2)}(\tau = 0) = 0$. All this evidence confirms that CSI and BI violations are rooted in the quantum dynamics that involves a virtual state in a collective de-excitation in the quantum ladder of the dressed states.

A more quantitative reading of these results is given in Fig. 4(a–b), that shows slices in the landscapes along lines I and II of the rightmost panel of Fig. 3(a). The quantum correlations violating the CSI are found in the side peaks and beyond, being larger the farther from the peaks. The same feature is present in the BI violation, which furthermore tends to the maximum value allowed $B_\Gamma = 2\sqrt{2}$. Figure 4(c–d) show $g_\Gamma^{(2)}(\omega, \omega)$ and $g_\Gamma^{(2)}(\omega, -\omega)$ —that can be used to derive $R_\Gamma(\omega, -\omega)$ and an approximation of $B_\Gamma(\omega, -\omega)$ [44]—as calculated exactly (solid red lines) [34, 41] and through the auxiliary multi-mode approximation used in previous works (dashed blue) [25, 26]. In the multi-mode approximation, the estimation is local around the peaks, that is, at $\omega/\omega_S = \pm 1$ and 0 (dotted vertical lines), where it is seen to be fairly accurate indeed, although not numerically exact. It can still lead to qualitative error, e.g., the autocorrelation at the sidebands is exactly zero in this approximation, predicting arbitrary violation of the CSI even when it is obeyed and an unphysical violation of the BI. A violation of the Bell’s inequality in these terms was predicted in Ref. [42]. However, the violation was considered ill-defined due to the perfect antibunching of the sidebands. Furthermore, these expressions are found in limiting cases for the filter linewidths: either $\Gamma \ll \gamma_\sigma \ll \Omega$ or $\gamma_\sigma \ll \Gamma \ll \Omega$. Both assume that the peaks are well separated to allow for the multiple-mode approximation. They predict no CSI or BI violation for narrow filters, which is ultimately verified although it is for values of the detector linewidth so small that they are unphysical. Solid lines in Fig. 5(a) show the dependence of R_Γ and B_Γ on the detector linewidth

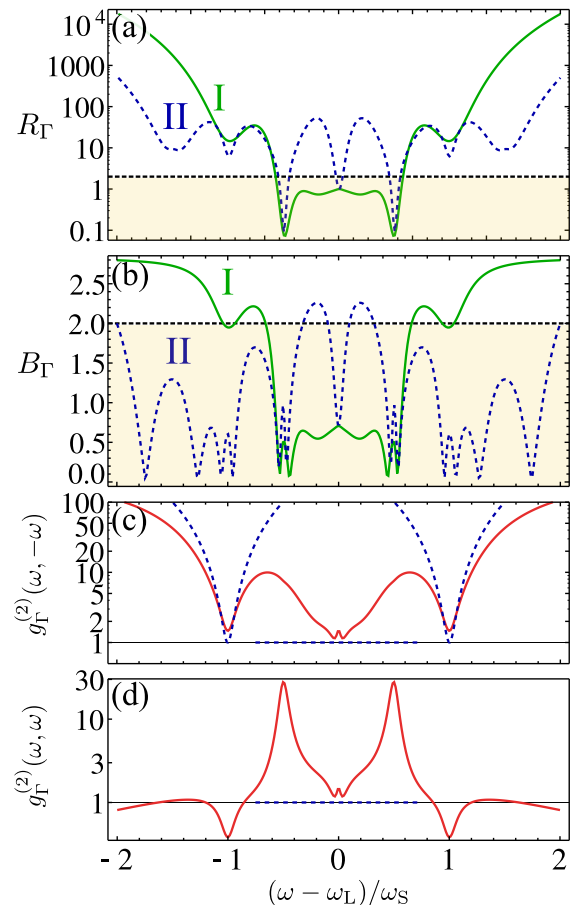


FIG. 4: (Color online) (a–b): Cuts of R_Γ (a) and B_Γ (b) along the lines I ($\omega, -\omega$) and II ($\omega, \omega_S - \omega$) of Fig. 3(a). (c–d): photon-correlation $g_\Gamma^{(2)}(\omega, \pm\omega)$ computed exactly (solid red) or through the usual multiple-mode approximation (dashed blue). In panel (d), the absence of the latter curve in some domains correspond to values which are, incorrectly, exactly zero (the vertical axis is in log-scale).

Γ for the three sets of frequencies $(\omega_i, -\omega_i)$, $i \in 1, 2, 3$ depicted in Fig. 5(b). For the already extremely small value of frequency windows $\Gamma = 0.1\gamma_\sigma$, the CSI and BI can be violated, in contradiction with the prediction of the multiple-mode approximation.

There are mainly three regimes of frequency correlations: narrow filters, peak filtering and overlapping windows. While narrow filters better define the structure, as can be seen in Fig. 3, they also correspond to longer times of integration due to the time-frequency uncertainty and thus average out the correlations. A maximum is found when filtering in windows of the order of the peak linewidth or above, which is a welcomed result for an experimentalist. The overlap of the filters marks a change of trend in all the curves, due to a competition between various phenomena involving, for instance, various transitions as well as averaging over different types of interferences. Dashed lines in Fig. 5(a) show the value

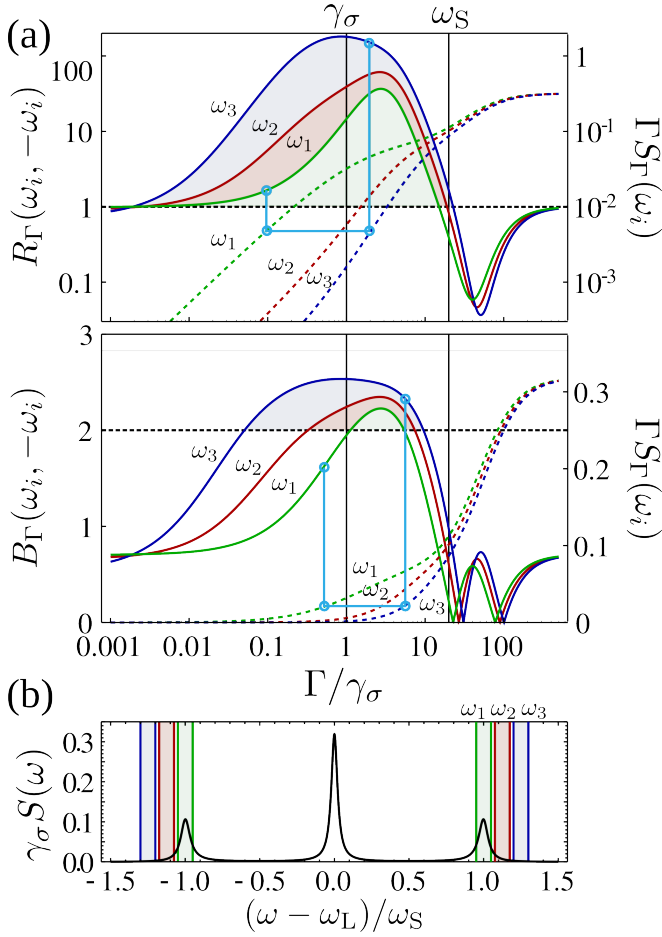


FIG. 5: (Color online) (a) Solid lines: $R_\Gamma(\omega_i, -\omega_i)$ (top panel) and $B_\Gamma(\omega_i, -\omega_i)$ (bottom panel) as a function of the detector linewidth for the three set of frequencies $(\omega_i, -\omega_i)$, $i \in 1, 2, 3$ depicted in panel (b). Dashed lines: Amount of signal $\Gamma S_\Gamma(\omega)$ that can be collected for the corresponding filter linewidth. Blue points illustrate how two configurations with the same amount of collected signal can yield different degrees of violation. (b) Resonance fluorescence spectrum, this time in linear scale, displaying the characteristic Mollow triplet and three sensors with linewidth $\Gamma = 2\gamma_\sigma$ centred at the frequencies used for panel (a): $\omega_1 = \omega_S$, $\omega_2 = 1.125\omega_S$ and $\omega_3 = 1.25\omega_S$. Parameters are the same as in Fig. 1.

of $\Gamma S_\Gamma(\omega)$ corresponding to the amount of signal that can be collected with a detector of linewidth Γ at the frequency ω [34]. This way, one can easily compare, for a given amount of available signal, the different degrees of violation which are accessible simply by selecting the frequency and the window of the detector appropriately. Since such correlations are useful for technological purposes, the ability to compute the entire landscape of frequency correlations becomes helpful for optimizing quantum information processing. Correlations along line I of the map arise from a well defined family of virtual processes, from which sideband correlations have been shown to be just a particular, and in fact also a detrimental case.

By positioning the filters away from the sidebands and increasing the frequency window of detection, it is possible to distill light showing stronger quantum correlations without paying any price on the signal.

CONCLUSIONS

We have shown how to evidence and optimize CSI and BI violations between photons resolved in frequency from a quantum source, with no constraints nor approximations from the theoretical description. Maximum violation is to be found not when correlating peaks in the spectrum, as previously thought, and thus linked to transitions between real states, but when involving virtual processes in the quantum dynamics. These results show the potential of frequency correlations to engineer quantum correlations, and could be applied towards the design of optimum quantum information processing devices.

ACKNOWLEDGEMENTS

We acknowledge the IEF project SQUIRREL (623708), the Spanish MINECO (MAT2011-22997, FPI & RyC programs) and the ERC PolaFlow.

* Electronic address: fabrice.laussy@gmail.com

- [1] R. Loudon, Rep. Prog. Phys. **43**, 913 (1980).
- [2] J. S. Bell, Rev. Mod. Phys. **38**, 447 (1966).
- [3] M. D. Reid and D. F. Walls, Phys. Rev. A **34**, 1260 (1986).
- [4] G. Hardy, J. Littlewood, and G. Pólya, *Inequalities* (Cambridge Mathematical Library, 1952), 2nd ed.
- [5] A. Aspect, Séminaire Poincaré **XVII**, 99 (2013).
- [6] A. K. Ekert, Phys. Rev. Lett. **67**, 661 (1991).
- [7] J. F. Clauser, Phys. Rev. D **9**, 853 (1974).
- [8] A. Aspect, P. Grangier, and G. Roger, Phys. Rev. Lett. **47**, 460 (1981).
- [9] A. Aspect, J. Dalibard, and G. Roger, Phys. Rev. Lett. **49**, 1804 (1982).
- [10] M. A. Rowe, D. Kielpinski, V. Meyer, C. A. Sackett, W. M. Itano, C. Monroe, and D. J. Wineland, Nature **409**, 791 (2001).
- [11] A. Kuzmich, W. P. Bowen, A. D. Boozer, A. Boca, C. W. Chou, L.-M. Duan, and H. J. Kimble, Nature **423**, 731 (2003).
- [12] V. Balać, D. A. Braje, P. Kolchin, G. Y. Yin, and S. E. Harris, Phys. Rev. Lett. **94**, 183601 (2005).
- [13] J. K. Thompson, J. Simon, H. Loh, and V. Vuletić, Science **313**, 74 (2006).
- [14] H. Sakai, T. Saito, T. Ikeda, K. Itoh, T. Kawabata, H. Kuboki, Y. Maeda, N. Matsui, C. Rangacharyulu, M. Sasano, et al., Phys. Rev. Lett. **97**, 150405 (2006).
- [15] A. M. Marino, V. Boyer, and P. D. Lett, Phys. Rev. Lett. **100**, 233601 (2008).

- [16] K. V. Kheruntsyan, J.-C. Jaskula, P. Deuar, M. Bonneau, G. B. Partridge, J. Ruaudel, R. Lopes, D. Boiron, and C. I. Westbrook, *Phys. Rev. Lett.* **108**, 260401 (2012).
- [17] B. Srivathsan, G. K. Gulati, B. Chng, G. Maslennikov, D. Matsukevich, and C. Kertsiefer, *Phys. Rev. Lett.* **111**, 123602 (2013).
- [18] H. J. Kimble and L. Mandel, *Phys. Rev. A* **13**, 2123 (1976).
- [19] E. B. Flagg, A. Muller, J. W. Robertson, S. Founta, D. G. Deppe, M. Xiao, W. Ma, G. J. Salamo, and C. K. Shih, *Nat. Phys.* **5**, 203 (2009).
- [20] O. Astafiev, A. M. Zagoskin, A. A. A. Jr., Y. A. Pashkin, T. Yamamoto, K. Inomata, Y. Nakamura, and J. S. Tsai, *Science* **327**, 840 (2010).
- [21] P. Lodahl, S. Mahmoodian, and S. Stobbe, arXiv:1312.1079 (2013), URL <http://arxiv.org/abs/1312.1079>.
- [22] B. R. Mollow, *Phys. Rev.* **188**, 1969 (1969).
- [23] C. Cohen-Tannoudji and S. Reynaud, *Phil. Trans. R. Soc. Lond. A* **293**, 223 (1979).
- [24] P. A. Apanasevich and S. Y. Kilin, *J. Phys. B.: At. Mol. Phys.* **12**, L83 (1979).
- [25] C. A. Schrama, G. Nienhuis, H. A. Dijkerman, C. Steijsiger, and H. G. M. Heideman, *Phys. Rev. A* **45**, 8045 (1992).
- [26] G. Nienhuis, *Phys. Rev. A* **47**, 510 (1993).
- [27] A. Aspect, G. Roger, S. Reynaud, J. Dalibard, and C. Cohen-Tannoudji, *Phys. Rev. Lett.* **45**, 617 (1980).
- [28] A. Ulhaq, S. Weiler, S. M. Ulrich, R. Roßbach, M. Jetter, and P. Michler, *Nat. Photon.* **6**, 238 (2012).
- [29] H.-P. Breuer and F. Petruccione, *The Theory of Open Quantum Systems* (Oxford Univ. Press, 2002).
- [30] E. del Valle and F. P. Laussy, *Phys. Rev. Lett.* **105**, 233601 (2010).
- [31] G. W. Gardiner and P. Zoller, *Quantum Noise* (Springer-Verlag, Berlin, 2000), 2nd ed.
- [32] L. Knöll and G. Weber, *J. Phys. B.: At. Mol. Phys.* **19**, 2817 (1986).
- [33] J. D. Cresser, *J. Phys. B.: At. Mol. Phys.* **20**, 4915 (1987).
- [34] E. del Valle, A. Gonzalez-Tudela, F. P. Laussy, C. Tejedor, and M. J. Hartmann, *Phys. Rev. Lett.* **109**, 183601 (2012).
- [35] M. B. Plenio and P. L. Knight, *Rev. Mod. Phys.* **70**, 101 (1998).
- [36] E. del Valle, *New J. Phys.* **15**, 025019 (2013).
- [37] R. J. Glauber, *Phys. Rev.* **130**, 2529 (1963).
- [38] J. F. Clauser, M. A. Horne, A. Shimony, and R. A. Holt, *Phys. Rev. Lett.* **23**, 880 (1969).
- [39] R. Loudon, *The quantum theory of light* (Oxford Science Publications, 2000).
- [40] A. G. Tudela, B. Silva, C. Sanchez Muñoz, E. del Valle, and F. P. Laussy, (in preparation) (2014).
- [41] A. Gonzalez-Tudela, F. P. Laussy, C. Tejedor, M. J. Hartmann, and E. del Valle, *New J. Phys.* **15**, 033036 (2013).
- [42] A. Joshi and S. V. Lawande, *Phys. Rev. A* **44**, 716 (1991).
- [43] N. A. Ansari, *Phys. Rev. A* **55**, 1639 (1997).
- [44] An approximation for $B_{\Gamma}(\omega, -\omega)$ can be obtained by dropping the last two terms of the numerator in Eq.(17) [43]. This approximation can be applied as long as there are no second-order transfer of photons between the modes, but these terms could be important in other cases. We have verified that they are indeed negligible in our configuration.